Annals of Nuclear Energy 213 (2025) 111102



Contents lists available at ScienceDirect

Annals of Nuclear Energy

journal homepage: www.elsevier.com/locate/anucene





Coupled STH/CFD calculations in support of the upcoming CIRCE-THETIS Experimental Campaign

Pietro Stefanini [a,*], Andrea Pucciarelli [a], Ivan Di Piazza [b], Daniele Martelli [b], Nicola Forgione [a]

[a] Università di Pisa, Dipartimento di Ingegneria Civile e Industriale, Largo Lucio Lazzarino 2, 56122, Italy
[b] Italian Agency for New Technologies, Energy and Sustainable Economic Development (ENEA), Brasimone Research Centre, 40032 Camugnano (Bologna), Italy

ARTICLE INFO

Keywords:
LMFR
Liquid Metal Reactors
LBE
CFD
STH
Coupling
Thermal-hydraulic

ABSTRACT

In the challenge of sustainable energy development, Liquid Metal Fast Reactors (LMFRs) offer a promising solution, utilizing liquid metal coolant for enhanced safety and efficiency. As the world addresses climate change and energy security, LMFR research gains significance, with ongoing projects aiming to accelerate development and deployment.

Within the EU PATRICIA project, an experimental campaign at ENEA Brasimone RC will further investigate LMFR technology using the updated CIRCE-THETIS facility. This effort focuses on improving the understanding of thermal–hydraulic behaviour of LBE cooled pool type reactors, during Protected Loss Of Flow Accident (PLOFA) scenarios, with a specific emphasis on the cooling capability provided by the Reactor Vessel Air Cooling System (RVACS) and the Helical Coil Steam Generator (HCSG).

Previous research conducted at the University of Pisa demonstrated that the most effective approach for the numerical analysis of the addressed PLOFA is the coupling method. This technique combines System Thermal Hydraulic (STH) and Computational Fluid Dynamics (CFD) approaches, aiming to overcome the weaknesses inherent in each method while exploiting their advantages.

In this study, a STH/CFD coupling scheme is developed for the pre-test analyses of some selected PLOFA scenarios in the CIRCE-THETIS facility. Our analyses primarily focus on assessing the effectiveness of the cooling strategy, with particular attention to the onset of natural circulation and the potential occurrence of dangerous peak temperatures during these transient events.

Our results indicate that all the adopted cooling strategies show sufficient capabilities to safely cool the system, highlighting the excellent heat removal capability of the RVACS. This research underlines the importance of the coupling approach in optimizing experimental setups and advancing the understanding of LMFR technology for sustainable energy production.

1. Introduction

In the challenge for sustainable and efficient energy sources, the Liquid Metal Fast Reactor (LMFR) stands out as an outstanding example of innovation and promise (GIF portal; IRSN, 2012). Exploiting the fundamental principles of nuclear fission, LMFRs represent a further step for power generation, offering potential for clean, reliable, and abundant energy production. As the world grapples with the challenges of climate change and energy security, the significance of LMFR research and development cannot be underestimated.

LMFRs are distinguished by their utilization of liquid metal, typically sodium or lead, as a coolant instead of traditional water-based systems. This revolutionary design not only should enhance safety and efficiency but also enable higher operating temperatures and greater fuel utilization, maximizing energy output while minimizing waste. Moreover, the inherent stability and heat capacity of liquid metal coolant mitigate the risk of core meltdown, addressing longstanding concerns associated with conventional reactor technologies.

By providing a reliable source of carbon-free electricity, LMFRs provide a viable alternative to fossil fuels, offering a pathway towards decarbonization and combating climate change. Furthermore, their scalability and adaptability make them well-suited for a variety of applications, from large-scale power generation to remote off-grid communities, fostering energy independence and resilience.

* Corresponding author.
E-mail address: pietro.stefanini@phd.unipi.it (P. Stefanini).

https://doi.org/10.1016/j.anucene.2024.111102
Received 30 April 2024; Received in revised form 29 October 2024; Accepted 29 November 2024
Available online 9 December 2024
0306-4549/© 2024 The Author(s). Published by Elsevier Ltd. This is an open access article under the CC BY license (http://creativecommons.org/licenses/by/4.0/).

However, realizing the full potential of LMFRs requires concerted efforts in research, development, and deployment. Challenges such as material compatibility, regulatory frameworks, and public perception must be addressed to ensure the safe and responsible implementation of this innovative technology. For this reason, several projects have been launched (THINS; SESAME; MYRTE; PATRICIA,) during the past years to accelerate progress and maximize the benefits of LMFRs, thus also reinforcing the knowledge-sharing on a European, and furthermore, global scale.

Nuclear reactors, particularly pool-type designs, are complex systems where phenomena occur across various length scales. To effectively study these complex phenomena and depending on the aimed level of accuracy, it could be useful adopting a multi-scale simulation approach. This would allow the integrations of models, each one focusing on different scales, to provide a comprehensive understanding of the reactor behaviour. Traditional reactor simulations typically employ single-scale models that focus on specific phenomena, such as neutronics or thermal-hydraulics. However, these models often fail to account for the intricate interactions between processes occurring at different scales within the reactor. Consequently, in recent years, efforts have been directed towards developing Multi-Scale and/or Multi-Physics simulations. This innovative approach enhances the accuracy of calculations by incorporating models from various scales, thus providing a more realistic representation of the underlying phenomena. Additionally, it enables more precise predictions of reactor performance under both normal and transient conditions, aiding in the optimization of design and safety assessments.

For instance, multi-scale analyses have been employed for safety evaluations concerning the boron dilution accident in new light water-cooled small modular reactor (SMR) concepts (Sanchez-Torrijos et al., 2023). Furthermore, integrating a multi-scale approach in reactor vessel design can lead to improved descriptions and predictions of thermal–hydraulic phenomena within the reactor vessel. Examples of this include studies by (Zhang et al., 2020) and (Victor Hugo Sanchez-Espinoza, 2023), where the authors describe two promising methods for combining computational fluid dynamics (CFD) with sub-channel codes to create a more comprehensive and accurate simulation tool for reactor vessel analysis. The successful validation of these methods paved the way for further development and application of multi-scale coupling systems.

Focusing specifically on liquid metal-cooled reactors, multi-scale analyses provide valuable tools for assessing fuel assembly behaviour. For example, in (Cao, 2020), a multi-scale analysis was conducted using a coupling procedure between the ATHLET system code and the KMC-SUB-traC sub-channel code. This methodology was employed to evaluate the safety performance of the fuel assembly in the medium-power reactor M^2LFR-1000. A different methodology was adopted for analysing the upper plenum of the same reactor (Zou et al., 2020). In this case, the system thermal-hydraulics (STH) code ATHLET was coupled with the OpenFOAM CFD code to study the mixing behaviour during an unprotected loss of flow accident. Another study demonstrated the applicability of the coupling of sub-channel codes with CFD to investigate flow blockage effects in the upper plenum region of the MYRRHA reactor, providing critical insights for safety analysis (Hanrui Qiu et al., 2024).

Within the framework of the EU PATRICIA project (PATRICIA), a forthcoming experimental campaign is scheduled at the ENEA Brasimone RC to help the advancement of liquid metal technology for pool-type reactors. The chosen facility is an updated version of the CIRCE-pool named CIRCE-THETIS (Lorusso et al., 2021). In contrast to its predecessor, CIRCE-HERO (Pesetti et al., 2018), the updated configuration shows two principal modifications: the Main Coolant Pump (MCP) and the Steam Generator (SG). Firstly, the MCP will replace the argon injection system, providing a forced circulation regime by actively propelling the fluid. Additionally, the former Bayonetted tube SG was removed in favour of a more space-efficient helically coiled design. Additionally, the facility will be equipped with the Reactor Vessel Air Cooling System (RVACS), to study the heat removal capability of this component. This component will be installed around the top part of the CIRCE-pool. These modifications create a brand-new environment for the analysis of the thermal–hydraulic behaviour of pool-type reactors. During the experimental campaign, several Protected Loss Of Flow Accident (PLOFA) scenarios will be performed to address the capabilities of the HCSG (Helical Coil Steam Generator) and RVACS components. Key objectives include investigating the heat transfer capabilities of liquid metals, assessing different passive safety systems, and studying the occurrence of natural circulation phenomena within the pool. The main goal of this paper is to support the experimental set-up.

This paper represents a step further in the research conducted at the University of Pisa in support of the CIRCE-THETIS experimental campaign scheduled at the ENEA Brasimone RC (Lorusso et al., 2021). This study is part of the Work Package 11 of the PATRICIA project (PATRICIA), aimed at developing robust numerical schemes for analysing liquid metal pool-type reactors. In previous studies at the University of Pisa (Stefanini et al., 2023a; Stefanini et al., 2023b), preliminary analyses of the CIRCE-THETIS facility were conducted using two main approaches: System Thermal Hydraulic (STH) and Computational Fluid Dynamics (CFD), in search of the most effective method to replicate the key phenomena which could occur during the transient planned for this facility. The results of the performed analyses suggest that the coupled approach (Pucciarelli et al., 2021) should represent the best choice. Coupled STH/CFD calculations are indeed becoming more and more common in the LMFR research community owing to the challenges connected to the use of pool type reactors. For example, at the NRG, Petten a multi-purpose coupling tool, myMUSCLE, is under development (Uitslag-Doolard et al., 2023) with the goal of a standardization of the coupling process. Another example is the University of Pisa where the coupling approach was applied for thermal hydraulics analyses of the CIRCE-pool (Pucciarelli et al., 2020; Angelucci et al., 2017). A similar case is the SCK-CEN, in Belgium, where a novel implicit scheme was developed, and the validation is being performed based on the E-SCAPE test facility data (Toti et al., 2018) and also ENEA Brasimone RC is working on coupling with RELAP5 and CFX (Cioli Puviani et al., 2023). For a classification of the coupling schemes the reader is referred to (Zhang et al. 2020). LMFRs present the perfect scenario where coupling tools may provide the best results: the pool represents an intrinsically 3D environment and the STH 1D approach thus represents a strong limitation for the quality and reliability of calculations. CFD, on the other hand, can provide detailed information of such regions. A stand-alone CFD approach for the whole facility may require a too large computational effort, the contribution of the STH code may instead help in reducing the computational cost. Coupled STH/CFD calculations thus seem to allow for a suitable compromise between quality and computational time. The main goal of the present numerical activity is to provide information to experimentalists about the temperature and mass flow rate trends to be expected in the pool during the postulated transient searching for some criticalities and helping the experimental set up. From the preliminary results emerges that all the considered cooling strategies show a strong capability for heat removal, with the RVACS component reporting a particularly effective performance.

2. Facility description

CIRCE-THETIS is an integral facility aimed at investigating some of the most important thermal-hydraulics phenomena of Liquid Metal cooled reactors. The facility is composed of a stainless-steel vessel, named CIRCE, which hosts the components of the primary loop.

The CIRCE vessel is 8 m tall and collects about 80 tons of LBE. A scheme of the pool, its main components and the foreseen flow path is reported in Fig. 1. From the pool environment the cold LBE enters inside the primary loop starting from the Feeding Conduit (FC) in the bottom part of the pool. Then it flows upwards inside the Fuel Pins Simulator

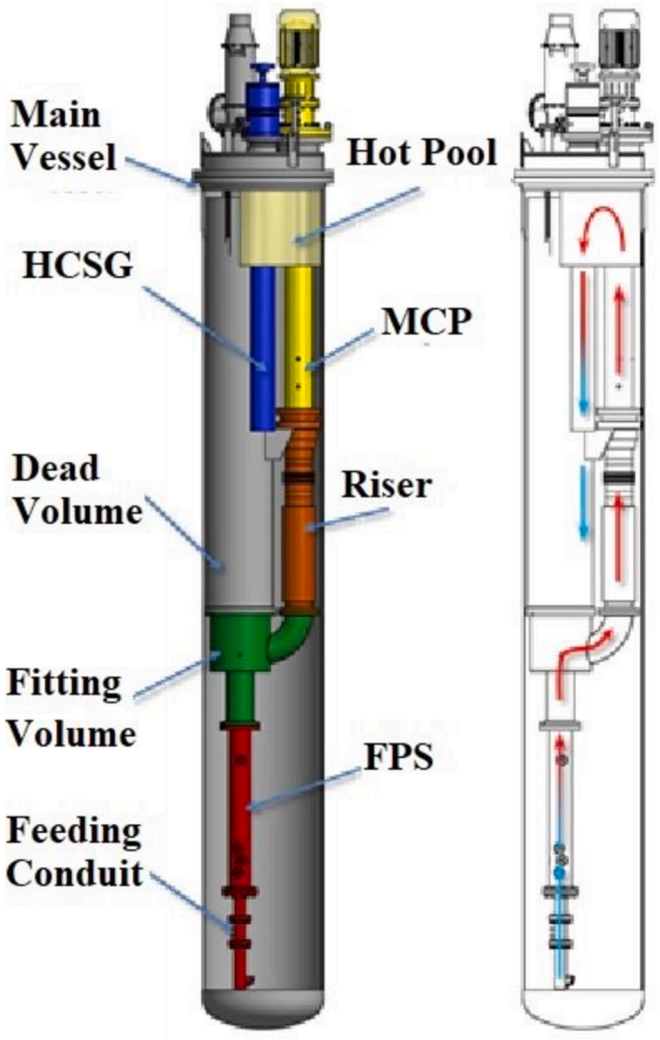


Fig. 1. CIRCE-THETIS scheme of the facility. .
Adapted from (Lorusso et al., 2021)

(FPS), where it is heated up, later moving towards the Fitting Volume (FV). From this latter region, the LBE flows inside the Riser and the Main Coolant Pump (MCP), which provides the prevalence for the forced circulation regimes, and continues towards the Hot Pool (HP). Here the hot LBE is collected and driven through the Helical Coiled Steam Generator (HCSG), where it is cooled by the water flowing in the secondary side's tubes before entering again into the pool.

Heat transfer is possible between the fluid flowing inside the internal components and the pool through the heat structures except for the HCSG and the Fitting Volume. In particular, it must be highlighted in this sense the relevant role of the pre-test numerical activities performed at the University of Pisa (Victor Hugo Sanchez-Espinoza, 2023) which encouraged experimentalists to recognize the need for a better insulation in the FV in order to prevent undesired heat losses at this very component. In the past, the CIRCE-pool was used in experimental campaigns adopting very similar configurations for the primary loop components (Pesetti et al., 2018). The MCP and the HCSG represent the very new features of this updated facility. The MCP is a mechanical pump which provides room for the forced circulation regimes. The Steam Generator (SG) is called THETIS (Thermal-hydraulic Helical Tubes Innovative System), and it has a very challenging geometry. The secondary side consists of 15 helical shaped tubes divided into three ranks running alternatively clockwise and counterclockwise, to enhance the mixing phenomena on the shell side (Lorusso et al., 2021), representing instead the primary side of the SG. The shell side of the SG is characterized by an annulus geometry: the central part hosts the feeding pipes of the helical tubes, here LBE is foreseen to be at rest. The water enters from the top part of the SG, flows inside the feeding pipes reaching the bottom part of the SG, and flows upward inside the helical tubes cooling the LBE which flows instead in the shell side. Fig. 2 reports an explicative section for this component.

The (Reactor Vessel Auxiliary Cooling System) RVACS component is positioned in the upper section of the facility, outside the pool, spanning nearly 4 m in length, and covering approximately half of the pool's total length. It consists of an annular chamber surrounded by insulation material, featuring four holes arranged orthogonally – two located at the upper section serving as inlets, and two positioned at the bottom serving instead as outlets. The vertical distance between outlets and inlets is 2.3 m and represents the active length of the component. Fig. 3 reports a scheme of the operational conditions and a CAD view of the component used for the CFD domain. RVACS components are foreseen in several LMFR concepts and are designed as additional cooling systems for accidental scenarios or decay heat removal.

2.1. Considered PLOFA

In the foreseen experimental campaign, four different cooling strategies for a Protected Loss Of Flow Accident (PLOFA) scenario will be investigated. All these scenarios simulate a failure of the Main Coolant Pump (MCP) followed by a scram of the reactor core. Consequently, the system experiences the transition from forced to natural circulation, while the power supply to the FPS is reduced to simulate the decay heat curve. The various cooling strategies will utilize two components: the RVACS and the HCSG, either individually or in combination. Three of the PLOFA scenarios will commence from the nominal steady state condition (whose operating conditions are summarized in Table 1), simulating the behaviour of a safe shutdown. The fourth PLOFA scenario will begin at the conclusion of the first PLOFA simulation, representing the transition from a safe shutdown regime to long-term cooling conditions.

Delving deeper into the PLOFA descriptions, during PLOFA1 the HCSG capability as a heat removal system is tested. From the nominal steady state conditions, the MCP is linearly turned off in 60 s and in the meanwhile the FPS power supply is reduced from 100 % to 13 %. The feedwater supply to the HCSG is reduced to the 10 % of the nominal value, while the RVACS is kept turned-off. Once new steady-state conditions are achieved, the PLOFA2 begins. At this stage, the HCSG is turned off and the RVACS is triggered simulating the long-term cooling condition. PLOFA3 and 4 again start from the nominal condition and simulate safe shutdown conditions. The PLOFA4 uses only the RVACS as

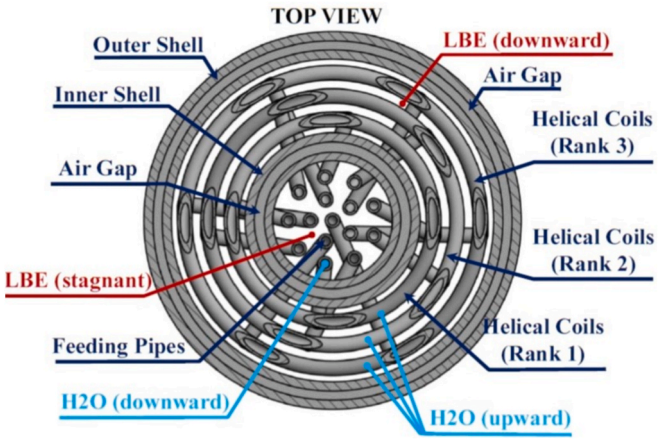


Fig. 2. THETIS scheme of the rank's subdivision. .
Adapted from (Lorusso et al., 2021)

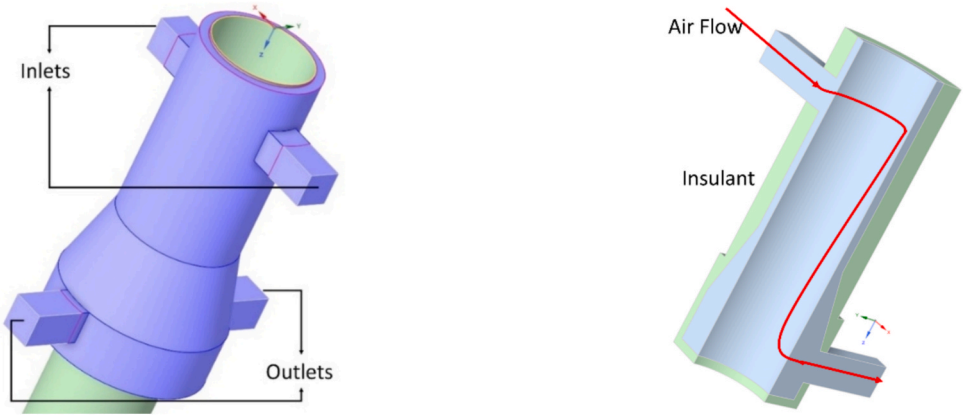


Fig. 3. RVACS scheme: on the left the CAD view, on the right 90 degrees section with a qualitative flow path of the air flow.

Table 1
Summary of the Boundaries for the Nominal Steady State.

Mass flow rate	35.17 kg/s
Power supply	450 kW
Power removed by the HCSG	400 kW
Foreseen thermal losses	50 kW

a heat sink while the PLOFA3 uses a combination of both RVACS and HCSG working together. The trends for the MCP and for the FPS remain the same of PLOFA1.

3. Developed numerical model

As anticipated, the performed preliminary analyses were addressed through the implementation of a coupling scheme, which integrates Computational Fluid Dynamics (CFD) and System Thermal Hydraulic (STH) approaches. In earlier analyses (Stefanini et al., 2023a; Stefanini et al., 2023b), it indeed became evident that neither STH nor CFD stand-alone applications may offer the most effective means of replicating the entire CIRCE system. Nevertheless, each one seems to provide suitable modelling capabilities for at least a part of the facility. Consequently, owing to the well-known RELAP5 capabilities, the STH approach is employed to address phenomena occurring on the secondary side where phase changes occur. Additionally, it serves to simulate the argon cover region above the free surface of the Lead-Bismuth Eutectic (LBE) without the need to introduce a Volume of Fluid (VOF) model in the CFD domain. The CFD simulated region covers instead the pool region, the internal components, the insulation and the RVACS as well. This strategic approach represents a good trade off between the number of interfaces considered for the coupling and the total cell count. It results in mitigation of the global computational load, which would otherwise be expensive, while assuring suitable modelling capabilities for each component of the facility.

3.1. RELAP5/Mod3.3 model

The adopted STH code is a modified version of RELAP5 (RELAP5 Code Manual, 2001), RELAP5/Mod3.3, developed at the University of Pisa to accommodate liquid metals as the working fluid which were not implemented in the original release of the code. Fig. 4 reports a snapshoot of the STH domain for the secondary side. In this context, the secondary side of the system (Pipe 220) was simulated using a single

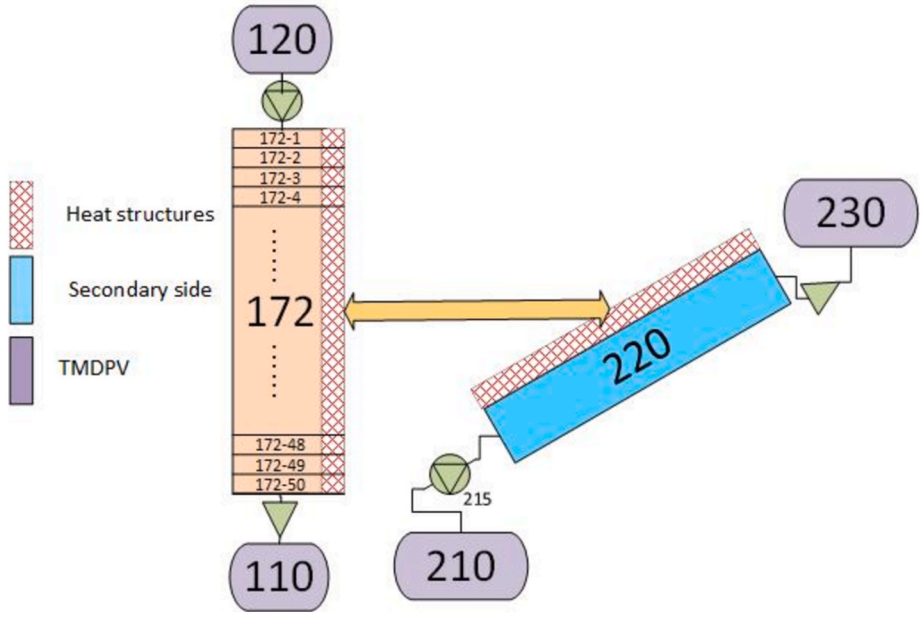


Fig. 4. Snapshoot of the STH domain nodalization. .
Adapted from (Stefanini et al., 2023)

inclined pipe having the equivalent cross section of the 15 helical tubes, with water flowing upwards. Boundary conditions were established using Time Dependent Volumes (TMDPVOL) at both the inlet (210) and outlet (220) of the pipe according to the addressed operating conditions. Mass flow is imposed at Time Dependant Junction 215.

Additionally, the inclined pipe was thermally connected to the primary side via heat structures. It Is worth noting that this geometry is known to enhance heat transfer (Santini et al., 2016; Hardik et al., 2015; Hardik and Prabhu, 2018) and RELAP5 has no specific correlations for helical tubes. Consequently, the STH model was adjusted to accommodate this increased heat transfer on the base of CFD and coupled STH/CFD evaluations by working on the thermal hydraulic diameter (Stefanini et al., 2023a). The observed heat transfer increment of about 10 % with respect to the simple pipe geometry is consistent with experimental measurement provided in the literature (Santini et al., 2016): the developed model was thus considered suitable for the present application as well. The primary side (Pipe 172) within the STH domain corresponds to the annular section of the SG's shell, where the LBE flows downward. Like the secondary side, boundary conditions were imposed using TMDPVOL s and a TMDPJUN (Time Dependent Junction) at the domain's ends (TMDPVOL 120, TMDPJUN 125 and TMDPVOL 110). When adopted in the coupled calculation, these boundaries conditions were updated on the base of the values provided by CFD. The exchanged power evaluated in this way by RELAP for the SG is later fed to the CFD as a volumetric heat source/sink providing the feedback for the coupling. Further considerations on the coupling scheme will be described in the following chapter.

3.2. ANSYS Fluent model

The adopted Computational Fluid Dynamics (CFD) code was ANSYS Fluent (version used Fluent 2022 R2) (ANSYS, Inc). A highly detailed geometry, inclusive of solid components, was employed within the CFD domain. This approach aimed to minimize user assumptions and enhance the realism of the problem under investigation. Given the preliminary nature of the study, conducted in support of an upcoming experimental campaign, the primary objective was to minimize user influence on the key phenomena within pool-type reactors. The mesh utilized consisted of polyhedral elements with a total cell count of 3.2 million. Wall refinement was incorporated to accurately resolve the boundary layer, 5-layer option at 30 % of the cell dimension was used. Fig. 5 illustrates a section of the mesh, highlighting the inflation. It can be noted that the mesh density within the insulator region was relatively coarse, as it experiences only conduction. This strategic approach allowed for computational resources to be conserved. Table 2 shows the maximum dimension selected during the mesh generation phase. It is important to note that the user sets the maximum dimension allowed and then the Fluent mesher adjusts the cells according to its internal requirement, trying to be as close as possible to the user setting. The results provided by the current approach were compared with previous calculations performed in the frame of a previous study adopting a more refined mesh (Stefanini et al., 2023a) returning very similar results. The mesh independence of the results is thus confirmed.

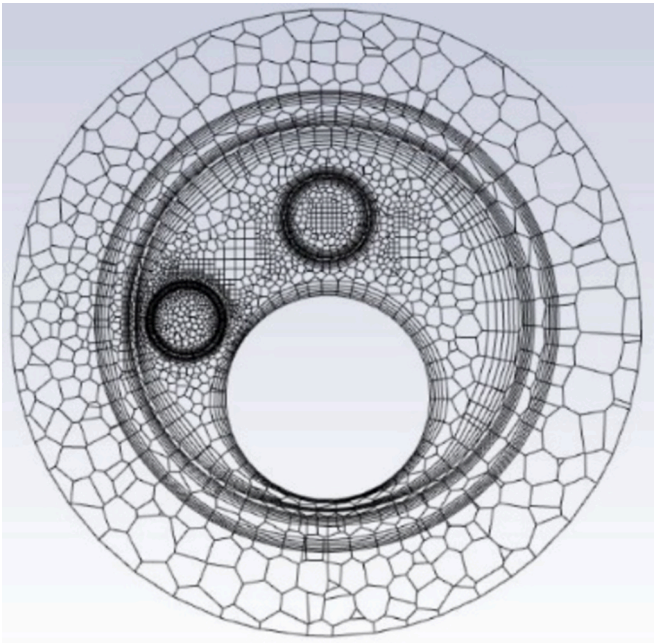


Fig. 5. Cross section of the adopted mesh.

The LBE was included in the Fluent library as a new working fluid implementing its properties as polynomial only functions of the temperature assuming pressure not to be relevant (NEA, 2015). The adopted turbulence model was the SST k-ω (Menter, 1994) with wall refinement treatment enabled: wall y + value is thus around 1 for all the surfaces. The turbulent Prandtl number was set constant and equal to 1.5 in agreement with several works in the available literature (Grishchenko et al., 2015; van Tichelen and Mirelli, 2017; Pucciarelli et al., 2020). The computational model employed a pressure-based solver utilizing an absolute velocity formulation. The pressure–velocity coupling was implemented using the "Coupled" method, with a "First-order Implicit" scheme applied for temporal discretization.

For the RVACS region, air was chosen as the working fluid. Given the absence of contact between different fluids in this area, the Volume of Fluid (VOF) model could be omitted, resulting in savings in computational efforts. Fig. 6 shows the scheme of the regions in the CFD domain.

The porous medium option was activated for the FPS, MCP, and HCSG to account for pressure drops within these regions while saving computational time. Particularly, the following components were not modelled in detail, their contributions to pressure drops were thus modelled via porous media: rods and spacers in the FPS, the impeller in the MCP, the helical tubes in the SG. Suitable pressure drop coefficients were tuned basing of higher fidelity calculations (see e.g. (Stefanini et al., 2023b). In addition, in the MCP region, a volumetric momentum source was included to replicate the influence of the pump during forced circulation. Eventually, a volumetric heat source was incorporated into the FPS region to represent the power supplied in that area. Particular attention must be paid to the the HCSG region. Since the HCSG represents an interface between CFD and the STH code in the considered coupled application, this region was subdivided into 50 parts, to match the STH nodalization. For each part a volumetric heat sink was considered; its value was defined on the basins of a parallel STH calculation. To model the heat losses towards the environment, a convective boundary condition was applied to the external surface of the insulation material. This condition assumed a heat transfer coefficient of 10 W/m^2K, representative of natural convection in air, and an environmental temperature of 30 °C.

Regarding the solid components of the domain, different material properties were applied depending on the specific component under consideration. For instance, stainless steel was utilized for the Feeding Conduit, the Hot Pool, the CIRCE vessel, and the Main Coolant Pump. For the Riser and Fitting Volume, an insulating material with thermal properties similar to rock wool was employed. The external insulation

Table 2
Cell dimension per region.

Region	Max Dimension [mm]
LBE-Pool	128
LBE-Loop	20
Air	50
Steel	8
Insulant	200

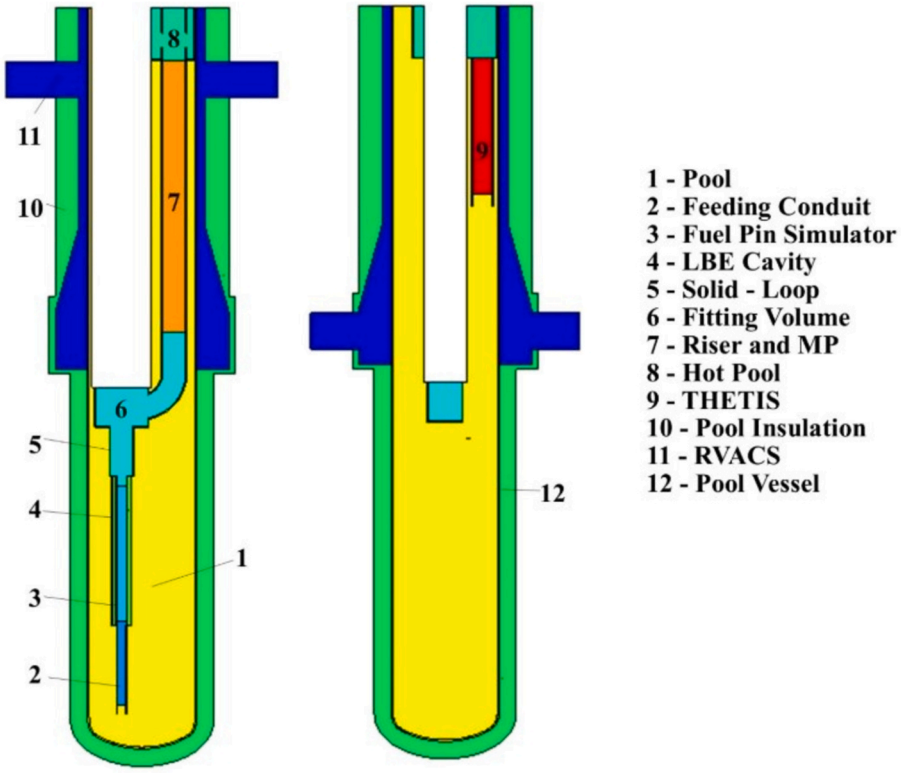


Fig. 6. Region subdivision in the CFD domain.

required a specific treatment and was divided into three sections: the first section extended from the bottom of the pool up to the bottom of the RVACS, the second section encompassed the RVACS, and the final section covered the top part of the pool. In these three regions, three different thermal conductivity coefficients were used. This approach was employed to obtain the wall temperature distribution measured by experimentalists during prior experimental campaigns involving the same Vessel-insulation configuration. Fig. 7 gives a snapshot of the different zones of the external insulant. The thermal property of the solid domain is given in the Table 3. The higher value of the insulant thermal conductivity adopted in the RVACS region is considered to account for the thermal bridges occurring in this very region owing to the presence of supporting metal structures immersed in the insulant material itself.

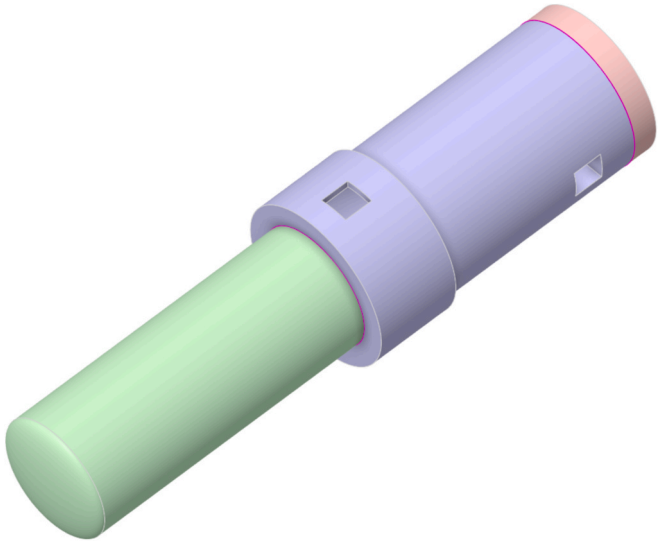


Fig. 7. External insulant subdivision.

3.3. Coupling section

A closer examination of the coupling process reveals that the two codes were interconnected via MATLAB as interface code, facilitating the exchange of information between them. Coupling occurs in two regions: the steam generator and the gas/liquid interface at the top of the pool.

At the architectural level, the coupling adopts a Partitioned model, employing an In-line coupling execution. This setup allows for mutual feedback between the codes, where the results from one code influence the solution of the other. Synchronization takes place at identical time steps, determined by the user, and information exchange occurs sequentially. This approach has been observed to enhance the stability of the calculation. An explicit numerical scheme was adopted, with both codes performing a once-through calculation from one synchronization point to the next, without conducting any convergence checks on the exchanged quantities at the interfaces. The spatial domains instead were overlapped for the HCSG region; the decomposition method was instead adopted for the Top pool. All the definitions provided in this section can be further explored in (Pucciarelli et al., 2021); Fig. 8 provides a graphical resume of the reported information.

3.3.1. The HCSG

An Overlapped Domain strategy was implemented for the HCSG region. Fig. 9 shows the considered geometries and the adopted information exchange processes. Both the primary and secondary sides of the steam generator (SG) were modelled in the system thermal-hydraulics (STH) domain, while only the primary side was represented in the computational fluid dynamics (CFD) domain. User-defined boundary conditions for the water side were based on the foreseen experimental matrix, while those for the primary side are set by the CFD results.

At each time step, the LBE mass flow rate and inlet temperature from the CFD model are extracted using MATLAB and fed into the STH code as boundary conditions. This allows the STH code to calculate the power removed in the HCSG, which is then used as a volumetric heat sink in the

Table 3
Solid material property.

	Insulant_bot	Insulant_mid	Insulant_top	Rock Woll	Stainless steel
Density [Kg/m^3]	75	75	75	75	8030
Cp [J/kgK]	1075	1075	1075	1075	502.48
Conductivity [W/mK]	0.15	2	0.55	0.035	16.27

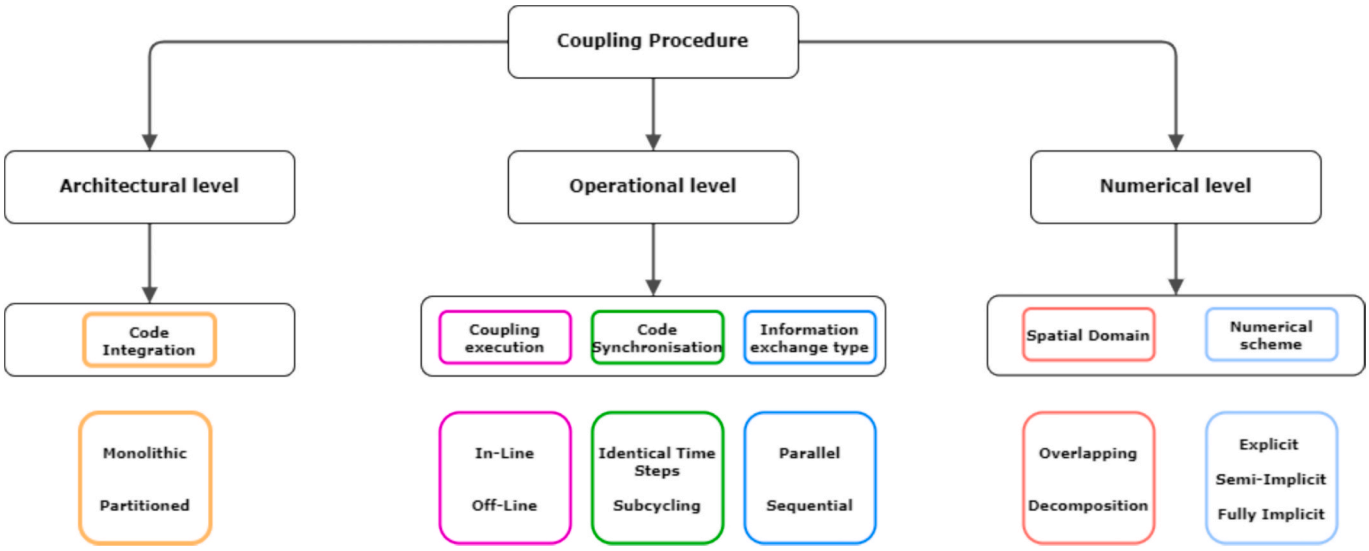


Fig. 8. Coupling scheme in the literature.

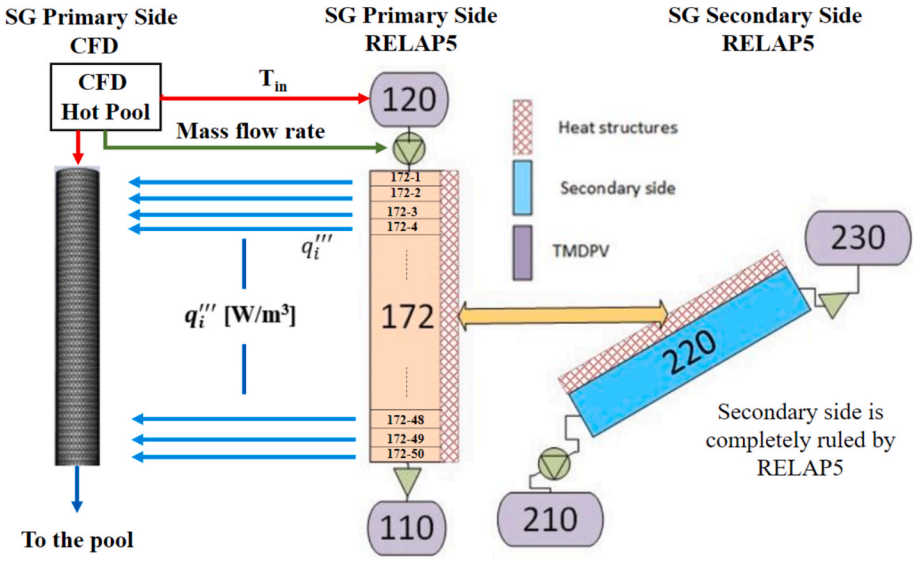


Fig. 9. Domain overlapping operational scheme.

CFD model for the corresponding time step. Recognizing the significance of the thermal barycentre in natural circulation, the SG domain was divided into 50 sub-volumes in both the STH and CFD models to enable a detailed analysis of the temperature distribution. The power removed in each sub-volume in the STH domain is linked to its corresponding CFD sub-volume as a heat sink, ensuring an accurate representation of the thermal behaviour of the system. Preliminary analyses indicated that most of the heat is removed in the initial (bottom) section of the SG, where water enters and phase change occurs from CFD to STH. In summary, the following information transfers occur:

- From CFD to STH:
  - LBE inlet mass flow rate
  - LBE inlet temperature
- From STH to CFD:
  - Power removed in each SG sub-volume section

3.3.2. *The top pool region*

This region posed the greatest challenge for the coupling. A domain decomposition technique was adopted. The free surface of the LBE is depicted in the STH domain through two vertical pipes (in Fig. 10, Pipe 4 and Pipe 11), representing the respective sections of the domain above

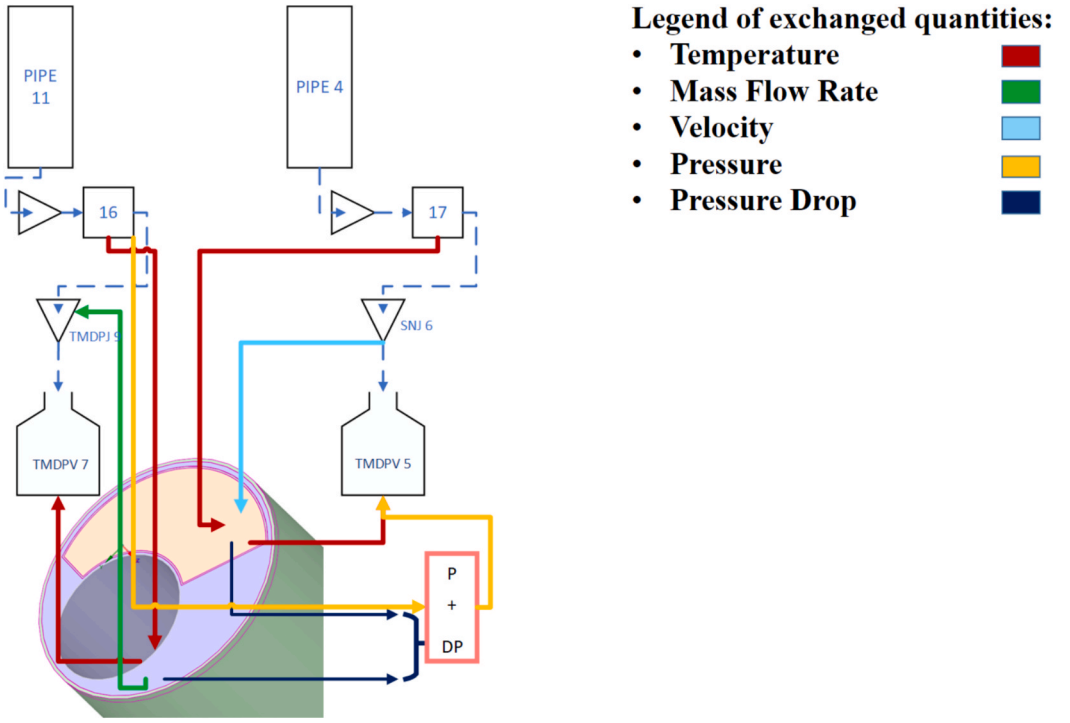


Fig. 10. Coupling scheme Top pool.

the Hot Pool and the Top Pool of the CFD domain. The information exchange scheme is provided in the following:

- From CFD to STH:
  - Temperature: At the inlet and outlet surfaces, used to set temperatures in TMDPVOL5 and TMDPVOL7.
  - Mass Flow Rate: at the CFD outlet section (Top Pool – violet surface), applied to TMPDJUN 9.
  - Pressure: to be set in TMPDVOL 5. This value comes as the result of the sum of the pressure calculated by RELAP5 in Single Volume (SNGLVOL) 16 and the pressure drops calculated by CFD between the inlet and outlet surfaces
- From STH to CFD:
  - Outlet Temperature (SNGLVOL 16): Used as the outlet temperature in reverse flow conditions for the Top Pool (violet surface).
  - Fluid Temperature (SNGLVOL 17): Applied at the velocity inlet of the CFD domain for the Hot Pool (okra yellow surface).
  - Fluid Velocity: Determined from SNGLJUN 6, applied at the CFD velocity inlet section (okra yellow surface).

This bidirectional exchange allows for a coherent and synchronized simulation, where both codes work together to represent the physical phenomena accurately.

4. Results

In this section the main considerations coming from the results for the PLOFA1, PLOFA2 and PLOFA 4 are discussed. PLOFA3 was not included since the main aim of the present work is the investigation of the cooling capabilities of the different devices in a stand-alone configuration. The primary focus of this analysis was the investigation of the temperature behaviour during the transient and the onset of natural circulation, aiming to identify potential hazardous situations that may arise for the selected operating conditions. This information will guide experimentalists in setting up instrumentation and measurements. Consequently, the time required for the system to reach its final cooled steady state was not a main concern, and the simulation was stopped as soon as the temperature behaviour clearly indicated a decreasing trend.

4.1. PLOFA 1

As mentioned above, the transient starts from nominal steady-state conditions, with the FPS and the HCSG operating at full capacity. The FPS is supplied with 450 kW of power, while approximately 400 kW of heat power is removed from the Steam Generator. The LBE's mass flow rate is 35.17 kg/s, imposed by the pump prevalence. Approximately 50 kW of energy is lost towards the environment. Fig. 11 displays two relevant sections of the pool under nominal steady state conditions. In the HCSG region, there is a relevant temperature drop in the LBE in correspondence of the outlet. This phenomenon is observable thanks to the axial subdivision of this region into sub-volumes which, as previously mentioned, allows for a better estimation of buoyancy forces. In this scenario, it is evident that the hotter LBE accumulates in the pool above the HCSG exit due to the absence of the LBE jet's mixing effect and thanks to buoyancy effects. Other relevant contributing factors to the heating of this region are the MCP and the Hot Pool. These components experience significant heat losses (approximately 20 kW in the MCP only) towards the pool due to lack of insulation. While this parameter will be fine-tuned once the actual facility will be operational, it serves as a concern for experimentalists. Pre-test analyses on this facility indeed already proved to be a fundamental tool for experimentalist: previous works highlighted heat losses from the FV regions to be a possible issue for the foreseen experimental campaign. Initial evaluations using CFD indicated heat losses of around 150 kW, this was considered unacceptable by experimentalists. Consequently, modifications were made to this component, implementing a double-wall geometry to provide insulation and address this issue: for sake of simplicity, in the present calculation, adiabatic walls are assumed for this component. In future analyses, a "real" geometry component will be introduced in the CFD domain once "as built" information will be released by experimentalists.

For PLOFA 1, the transient begins with a gradual reduction of the power supply to the FPS, linearly decreasing from 100 % to 13 % over a period of 60 s. Following a 1-second delay, the MCP is similarly turned

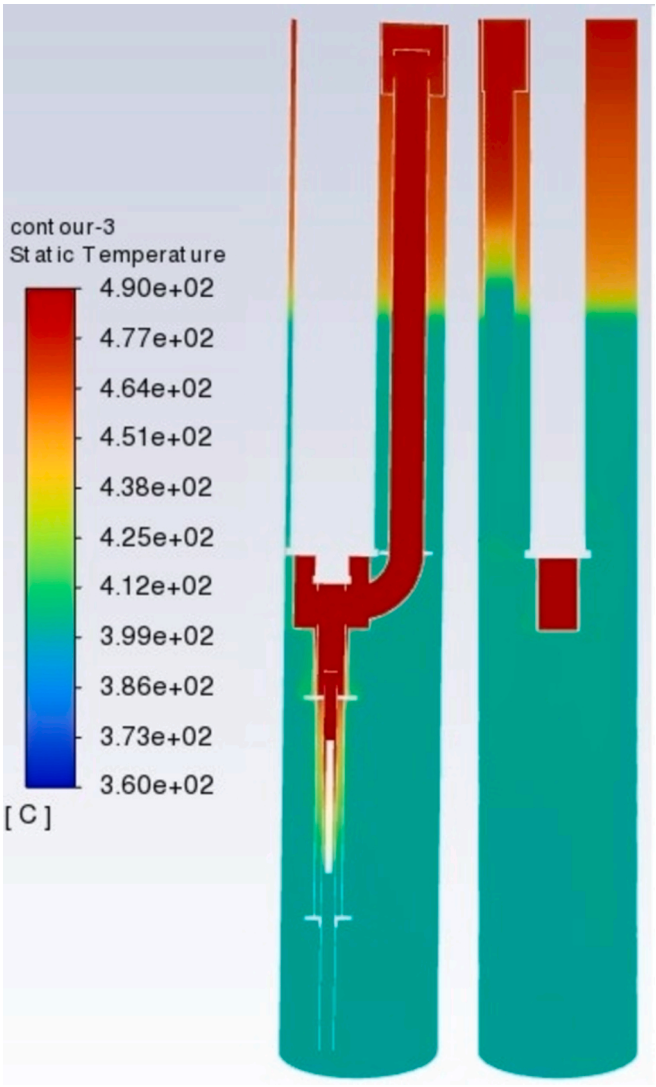


Fig. 11. Initial steady state conditions.

off with the same linear trend, simulating a pump failure. This delay was established as a safety measure to mitigate the risk of potential temperature spikes that could damage instrumentation and components. The feedwater supply, instead, follows a similar linear trend as in the FPS: in 60 s it reaches about the 20 % of the nominal value. Fig. 12 and Fig. 13 report the temperature trend and the mass flow rate trend inside the loop during the first 1500 s from the beginning of the transient, respectively. In Fig. 12, the temperature trends within the loop are depicted. Over the first 60 s, the temperature at the outlet of the FPS region (blue line) exhibits a linear decrease, primarily influenced by the reduction in power supply. On the other hand, the temperature at the inlet of the HSCG region (yellow line) displays a smoother reduction. It remains higher than the FPS outlet section for approximately 500 s due to the delay connected to the gradual propagation of the "cold wave" of LBE from the FPS region to the SG inlet section. The temperature reduction at the HCSG inlet section is delayed by several factors. Firstly, it takes approximately 100 s for the LBE to reach the steam generator inlet from the FPS outlet. Additionally, the decrease in temperature at the HCSG is significantly influenced by the thermal inertia of the Hot Pool. Eventually, since after the power decrease temperature is now higher in the pool than in the loop, the LBE in the loop is heated-up through the structures of the MCP and HP. At the outlet section (purple line), the LBE temperature initially increases by 40 degrees before starting to decrease again. This is attributed to two main factors: the reduction in feedwater supply on the secondary side and the timing of the cold wave reaching the bottom part of the SG. While the former acts in just 60 s, providing room for a temperature increase at the outlet section, the latter effect is experienced with some delay, and it is responsible for the subsequent decreasing part of the trend. The FPS inlet (red line) instead is the last to be affected by changes because of the thermal inertia of the pool; during the first 1500 s it can indeed almost be considered as constant. Cooling proceeds successfully for the whole transient: at the final steady-state the pool mean temperature decreased by about 50 °C with respect to the initial reference conditions.

Fig. 13 shows the mass flow rate trend in the loop. It can be seen clearly that, after the simulated pump failure, the transition from forced to natural circulation occurs. After 60 s from the beginning of the transient, when the pump is eventually completely stopped, the mass flow is about 10 kg/s. Later, it decreases reaching a minimum at about 400 s; when natural circulation is fully developed the final mass flow is in the range of about 8 kg/s. The observed flow rate reduction from an initial 35 kg/s to approximately 8 kg/s is primarily due to two key factors: the reduction in pump RPM, and the subsequent system inertia leading to a new equilibrium.

1. **Reduction in Pump RPM**: The initial sharp drop-in flow rate to about 10 kg/s is directly influenced by the reduction in the pump's RPM. As the pump speed decreases (i.e. the momentum source in the present calculation), the driving force for the flow diminishes,

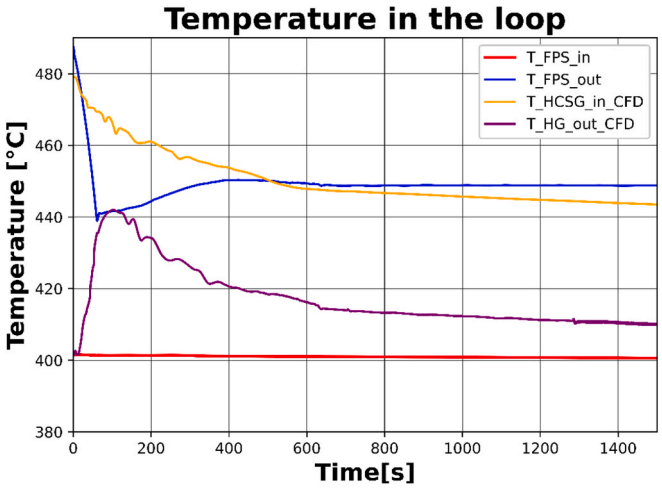


Fig. 12. Temperature trend during the transient PLOFA1.

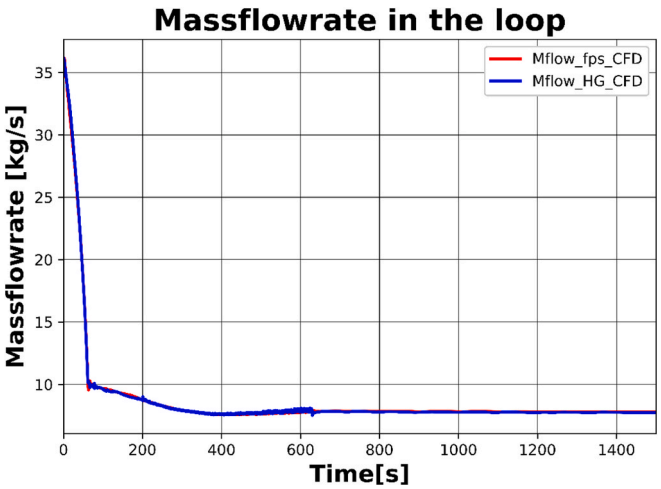


Fig. 13. Mass flow trend during the transient PLOFA1.

leading to an immediate decrease in the flow rate. This is a direct response to the mechanical adjustments in the pump's operation.

2. **Gradual Adjustment to New Equilibrium**: The flow rate further reduces to around 8 kg/s as the system seeks to achieve a new equilibrium. During this phase, the LBE flow adjusts to the reduced driving force and redistributes within the loop. The interplay between the pump's reduced capacity and the natural circulation leads to a gradual decrease in flow rate until a new equilibrium is established.

The final mass flow rate value, reached during natural circulation regime, allows for a suitable cooling of the system.

Fig. 14 illustrates contour plots of the pool temperature at different time points during PLOFA1. Initially, thermal stratification appears above the Steam Generator outlet. This region indeed experiences less and delayed influence from the cold LBE jet exiting the SG, also due to buoyancy effects. Another interesting observation can be made regarding the temperature distribution inside the steam generator. It is evident that most of the temperature change occurs in the bottom half of the component, close to the LBE outlet section. The water on the secondary side begins cooling the primary side from this point onward and reaches temperatures close to that of the LBE entering the HCSG before reaching the midpoint of the path, highlighting the high efficiency of this component. The other two sections in Fig. 14 depict the temperature distribution in the pool after 1500 s and the foreseen final steady state. In both cases, it is evident that the pool is effectively cooling, despite the presence of a "hot spot" still visible above the outlet section, as indicated by a noticeable change in the colour field. During the transient, both power and temperature are allowed to evolve naturally. The possible final steady state was determined through a standalone CFD calculation in which the power removed at the SG was fixed and set coherently with the one provided by a RELAP5 for the very same condition. In particular, the SG power estimation was achieved iteratively checking the power predicted to be removed by RELAP5 as a consequence of changes in the HCSG LBE inlet temperature. Once the inlet temperature achieved a new steady state, a fixed power removal was thus assumed in the CFD domain. In this scenario, it is expected that about 30 kW will be removed from the SG, while approximately 28 kW will be lost to the environment. It is noteworthy that the SG reaches the expected 30 kW removal rate within the first 1500 s.

4.2. PLOFA 2

As mentioned above, the foreseen final state of PLOFA1 was predicted via a steady-state calculation. The focus of this work is understanding the cooling capabilities of the devices and thus no evaluation of the time needed to achieve the final steady state was performed. In order to address the PLOFA1-PLOFA2 switch in a conservative way, an initial steady state with higher temperature was considered. The transition commences with a linear reduction of the feedwater supply, decreasing from 20 % of the nominal value to 0 % over 3 s. Simultaneously, the blower starts to inject air, increasing from 0 to 0.117 kg/s within the same 3 s. The selected air mass flow rate value was assumed in similarity with the preliminary estimation performed in the frame of a previous work performed at the University of Pisa(Stefanini et al., 2023b). Fig. 15 illustrates the temperature evolution of four relevant locations inside the CIRCE loop. Compared to PLOFA 1, the temperatures decrease smoothly, except for the temperature at the outlet of the Steam Generator (purple line), which experiences an increase due to the complete evaporation of water inside the secondary side tubes as a consequence of the simulated feedwater stop. It is evident that the RVACS component proves to be highly effective in cooling, leading to a new colder steady state.

It's also worth noting that the FPS inlet temperature experiences a higher cooling rate, contrary to the behaviour observed in PLOFA 1. This phenomenon can be attributed to the activation of the RVACS. While in

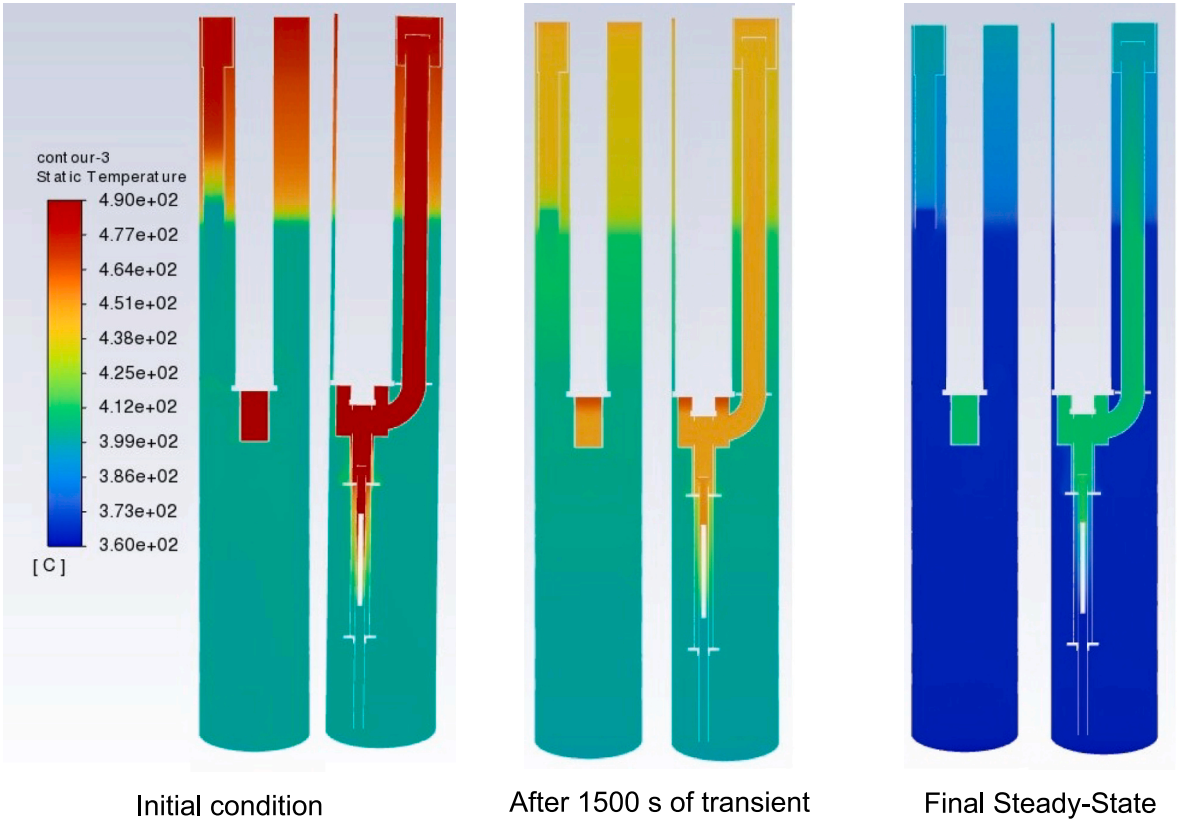


Fig. 14. Pool temperature distribution evaluated by the coupling scheme during the transient for PLOFA1.

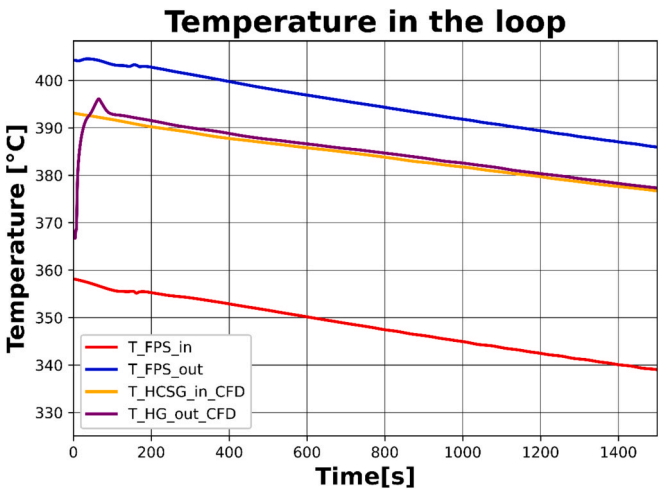


Fig. 15. Temperature trends during PLOFA2.

PLOFA1 cooling occurred only in the HCSG, in PLOFA2 the pool is directly cooled by the RVACS from the external side. The large size of the component seems very effective in cooling down the pool thus immediately affecting the temperature distribution also in the bottom part of the pool itself.

Fig. 16 displays the mass flow rate trend. No relevant phenomena occur with respect to the final steady-state conditions achieved at the end of PLOFA1 because the natural circulation is already settled: a little reduction in the mass flow rate of around 0.2 kg/s occurs as a consequence of the impairment of the buoyancy forces across the loop. This behaviour is in fact to be connected to the new position of the thermal barycentre provided by the new heat sink position. Nevertheless, as a matter of fact, the RVACS seems able to keep the system safely cooled.

Fig. 17 reports the section of the initial state for PLOFA2, after 1500 s from the beginning of the scenario and at the foreseen final steady state. Starting from the initial state, it is evident that some thermal stratification is present in the upper region of the pool. The reasons for this thermal stratification were already mentioned in the previous section but here it is interesting to notice that after 1500 s and, especially at the final steady state, the thermal stratification becomes weaker and weaker. The activation of the RVACS indeed affects this very region, cooling the LBE and providing for some convection that lowers the thermal effect due to the heat losses from the MCP region. Contrary to PLOFA1, here for the simulation of the final steady state no additional boundary conditions set by RELAP were used because the SG is simply

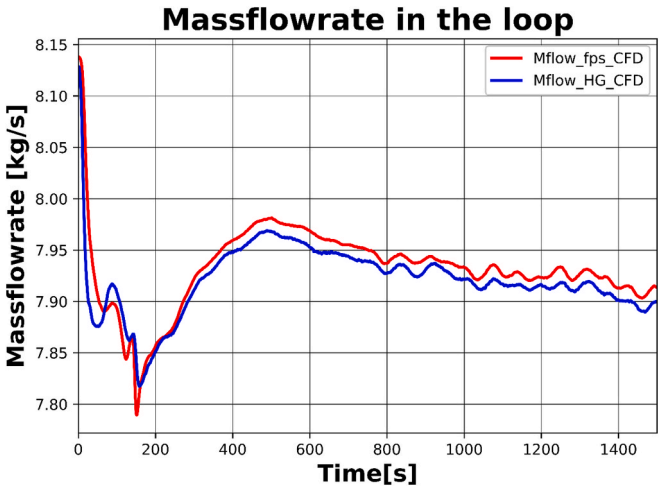


Fig. 16. Mass flow rate trend during the PLOFA2.

switched off and the RVACS is completely simulated in the CFD domain: the CFD stand-alone calculation is thus free to evaluate the final condition just with the design parameter since no power is exchanged at the HCSG. During this condition, the power removed from the RVACS is 18 kW which is very close to the design value of 22 kW.

4.3. PLOFA 4

In this transient, the RVACS serves as the safe shutdown cooling system. As in the PLOFA 1, the scenario considers similar behaviours regarding the MCP and the FPS. However, the activation of the SG and the RVACS differs from PLOFA1. At the start of the transient, the feedwater supply undergoes a linear reduction from 100 % to 0 % over 60 s. The RVACS reaches the 100 % of the selected flow rate over 3 s, 54 s after the beginning of the transient. It is here worth to mention that the temperature distribution in the pool during the initial steady state of the PLOFA4 is a bit different with respect to the one of PLOFA1. This difference is due to the needed change in the boundary conditions in the RVACS component. While for the PLOFA 1, the inlet and outlet of the air were set as walls since the RVACS was not active and was only considered for the thermal losses towards the environment, for the PLOFA4 these very same boundaries were used as proper inlet and outlet introducing additional heat losses towards the environment due to the use of the radiative model.

Fig. 18 illustrates the temperature trends within the loop for the specified PLOFA4. Similarly to PLOFA1, the gradual decrease in FPS power supply is clear in the outlet temperature of the FPS component (blue line) during the first phase of the PLOFA. Later, when the mass flow decreases owing to the start of natural convection (see Fig. 16), a relative maximum in the outlet FPS temperature is experienced accordingly. The LBE temperature at the inlet of the HCSG follows a similar reduction compared to the PLOFA1. The primary cause of the temperature reduction is attributed to the propagation of the cold LBE wave coming from the FPS, like in the previously mentioned case. In addition, during the initial part of the transient, the fluid in the top region of the pool is hotter than the one in the MCP and riser because of the FPS shut down; a partial heating of the fluid during its rise is to be considered leading to a longer delay for the temperature decrease to be experienced at the HCSG inlet. It is noteworthy to highlight the spike observed at the HCSG outlet temperature. This sudden increase is a result of the feedwater supply reduction; temperature is later temporarily reduced (first peak) due to the evaporation of the water still present in the tubes, before eventually reaching almost the same value as the SG inlet temperature (second peak).

In contrast to PLOFA1, where the FPS inlet temperature is affected much later in the transient, here, the FPS inlet temperature begins decreasing right from the onset of the transient. This is due to the direct influence of the RVACS activation on the entire pool environment, making the pool domain more sensible to cooling effects.

Fig. 19 displays the mass flow rate trend for this very same transient. No additional considerations emerge, the trends display a behaviour similar to the one of the PLOFA1. The first part is mainly driven by the linear reduction of the pump prevalence, then natural circulation is established.

Fig. 20 presents the same section as the other previous two cases: initial condition, after 1500 s from the transient start and the final steady state. Similarly to the PLOFA 2 case, the final steady state was simulated using a stand-alone CFD calculation.

In this instance, the dissipation of thermal stratification above the Steam Generator outlet section is even more pronounced. Beginning from the nominal steady state, where hot LBE accumulates in the top region of the pool, it is evident that the hot LBE gradually descends, cooled by the RVACS, until the final steady state is achieved, and thermal stratification almost completely disappears.

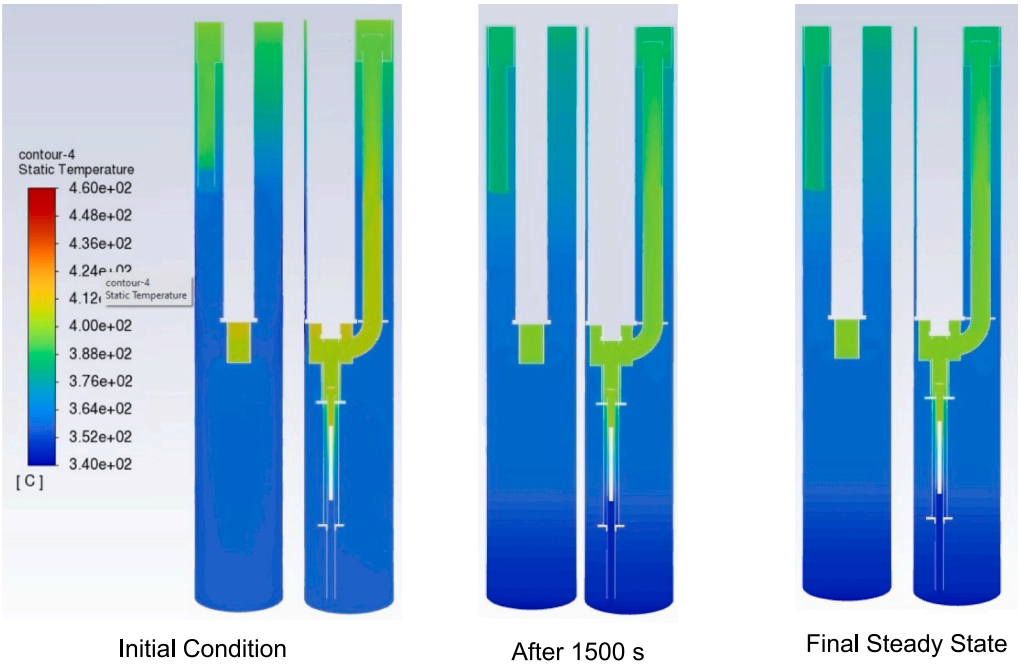


Fig. 17. Pool temperature distribution evaluated by the coupling scheme during the transient for PLOFA2.

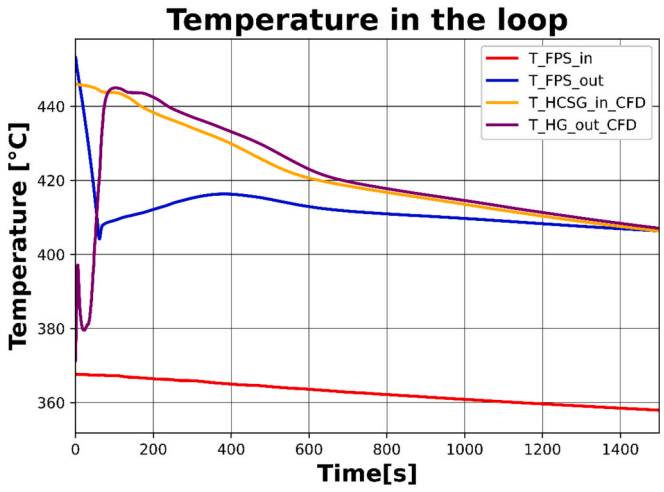


Fig. 18. Temperature trend during PLOFA4.

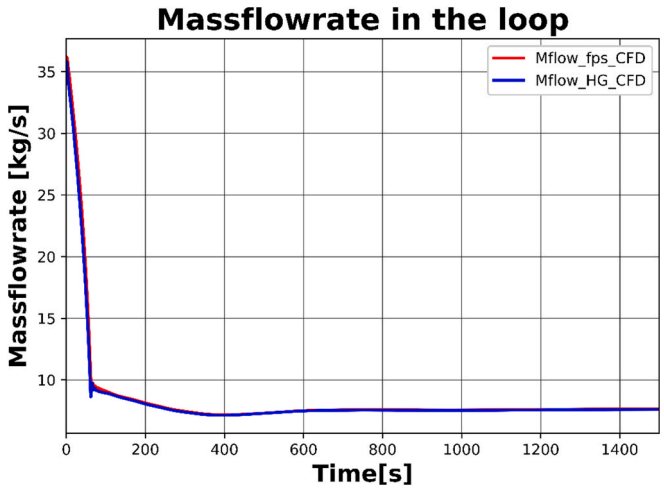


Fig. 19. Mass flow rate trend PLOFA4.

5. Conclusion

The focus of this work was the simulation of three postulated PLOFA foreseen for the experimental campaign that will be performed at the ENEA Brasimone RC in the frame of the PATRICIA project. The main goal was to find out possible harmful situations that could occur during the tests, providing information to the experimentalist for a better comprehension of such phenomena and allowing for a better experiment set up.

From a numerical point of view, a coupling STH/CFD method was developed and described here. The chosen codes were RELAP5/Mod3.3 and ANSYS Fluent, with MATLAB working as the interface code. The numerical scheme used was explicit while two different strategies were adopted for what concerns the spatial domain: decomposition method for the argon cover region and overlapped for the steam generator. This approach allows for the representation of the whole transient scenario even if, due to computational costs, just the first 1500 s of the transient were simulated. The final conditions were achieved with CFD stand-alone calculations imposing boundary conditions selected in accordance with the design parameters.

The obtained results showed that in all the considered scenarios a safe cold condition is reached, and no harmful situation occurs, all the temperatures remain in the safety range and the natural circulation is established and is sufficient for the cooling purpose. In addition, the activation of the RVACS reduces the thermal stratification in the top part of the pool affecting directly that region. As final remarks, all the considered cooling strategies seem to be “safe” enough and capable to cool the facility during a PLOFA scenario.

The paper thus supports the use of numerical activities, and especially coupled STH/CFD calculations, as suitable modelling tools for pre-test analyses in order to investigate safe and dangerous operating conditions. Thanks to the continuous improvements of STH, CFD and coupled STH/CFD applications modelling for liquid metal thermal-hydraulics, it is expected that such approaches will play a relevant role in the design and licensing of future LMFBRs.

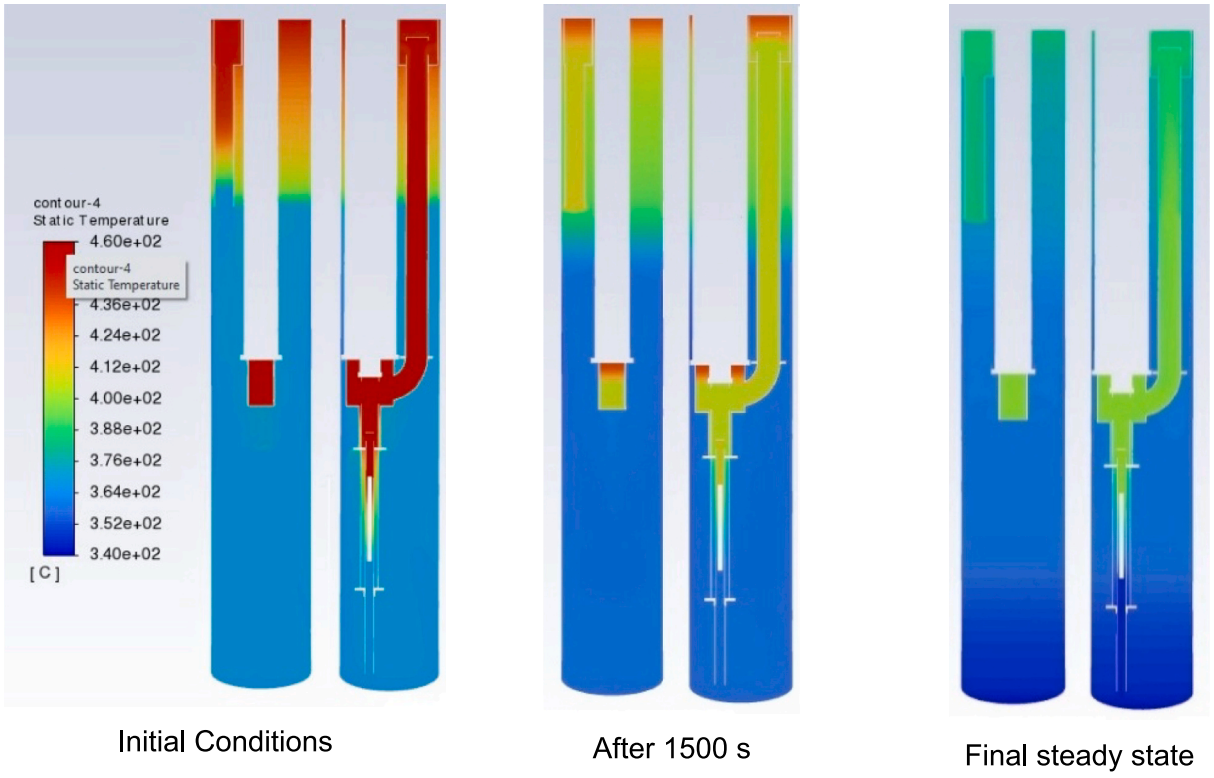


Fig. 20. Pool temperature distribution evaluated by the coupling scheme during the transient PLOFA4.

Declaration of competing interest

The authors declare that they have no known competing financial interests or personal relationships that could have appeared to influence the work reported in this paper.

Acknowledgement

This project has received funding from the Euratom research and training programme 2019-2020 under Grant Agreement No 945077 in the frame of the PATRICIA project.

Data availability

Data will be made available on request.

References

M., Angelucci, D., Martelli, G., Barone, I., Di Piazza, N., Forgione, "STH-CFD Codes Coupled Calculations Applied to HLM Loop and Pool Systems, Science and Technology of Nuclear Installations, Volume 2017, Article ID 1936894, 13.

ANSYS, Inc., "ANSYS Fluent User's Guide, Release 19.2", August 2018.

Liankai Cao, Xilin Zhang, Hongli Chen, "Sub-channel-based multiscale thermal-hydraulic analysis of a medium-power, lead-cooled fast reactor" DOI: 10.1002/er.5279. 2020.

Cioli Puviani, P., Zanino, R., Del Moro, T., Giannetti, F., Gonfiotti, B., Di Piazza, I., Martelli, D., Tarantino, M., 2023. CFD – STH Code Coupling for the Thermal Hydraulic Analysis of NACIEUP Experimental Facility. NURETH20. https://doi.org/10.13182/NURETH20-40088.

GIF portal, https://www.gen-4.org/gif/.

Grishchenko D., Jeltsov M., Kööp K., Karbojian A., Villanueva W., Kudinov P., 2015. "The TALL-3D facility design and commissioning test for validation of coupled STH and CFD codes", Nucl. Eng. Des. 290, 144-153.

Hanrui Qiu, Mingjun Wang, Jing Zhang, Wenxi Tian, G.H. Su, "Multi-scale coupling analysis of the flow blockage accident in the typical LFR", International Journal of Thermal Sciences, 195 2024 108615.

Hardik, B.K., Prabhu, S.V., 2018. Heat transfer distribution in helical coil flow boiling system. Int. J. Heat Mass Transf. 117, 710–728.

Hardik, B.K., Baburajan, P.K., Prabhu, S.V., 2015. Local heat transfer coefficient in helical coils with single phase flow. Int. J. Heat Mass Transf. 89, 522–538.

IRSN, 2012, "Overview of Generation IV (GENIV) Reactor Designs, Safety and Radiological Protection Considerations.", IRSN Report 2012/158.

P. Lorusso, I. Di Piazza, D. Martelli, A. Musolesi, M. Tarantino, 2021. "Preliminary design of THETIS test section for the CIRCE facility", ENEA report, Ref CI-I-R3534.

Menter, F.R., 1994. Two-equation eddy-viscosity turbulence modelling for engineering applications. AIAA J. 32 (8), 1598–1605.

MYRTE, http://myrte.sckcen.be/.

NEA, Nuclear Energy Agency, Handbook on Lead-bismuth Eutectic Alloy and Lead Properties, Materials Compatibility, Thermal hydraulics and Technologies, NEA No. 7268 © OECD 2015.

PATRICIA, https://patricia-h2020.eu/.

A. Pesetti, N. Forgione, V. Narcisi, P. Lorusso, F. Giannetti, M. Tarantino, 2018, "ENEA CIRCE-HERO test facility: geometry and instrumentation description", ENEA report for Project H2020 SESAME WP5.2, Ref CI-I-R-343.

Pucciarelli A., Toti A., Castelletti D., Belloni F., Van Tichelen K., Moscardini M., Galleni F., Forgione N., "Coupled system thermal Hydraulics/CFD models: General guidelines and applications to heavy liquid metals", 2021, 153 107990.

Pucciarelli, A., Galleni, F., Moscardini, M., Martelli, D., Forgione, N., December 2020. STH/CFD coupled calculations of postulated transients from mixed to natural circulation conditions in the NACIE-UP facility. Nucl. Eng. Des. 370 (15). https://doi.org/10.1016/j.nucengdes.2020.110913.

Pucciarelli, A., Galleni, F., Moscardini, M., Martelli, D., Forgione, N., 2020. STH/CFD Coupled Simulation of Protected Loss of Flow Accident in the CIRCE-HERO Facility. Appl. Sci. 10, 7032. https://doi.org/10.3390/app10207032.

RELAP5 Code Manual, 2001, "RELAP5/Mod3.3 code manual Volume I: Code structure, System models and solution methods". Nuclear Safety Analysis Division; Information System Laboratories, Inc., Rockville, Maryland Idaho Falls, 2001.

Sanchez-Torrijos, J., Zhang, K., Queral, C., Imke, U., Sanchez-Espinoza, V.H., 2023. Multiscale analysis of the boron dilution sequence in the NuScale reactor using TRACE and SUBCHANFLOW. Nuclear Eng. Des. 415, 112708.

Santini, L., Cioncolini, A., Butel, T.M., Ricotti, E.M., 2016. Flow boiling heat transfer in helically coiled steam generator for nuclear power applications. Int. J. Heat Mass Transf. 92, 91–99.

SESAME, http://sesame-h2020.eu/.

Stefanini, P., Pucciarelli, A., Forgione, N., Di Piazza, I., Martelli, D., 2023. Numerical analyses of the CIRCE-THETIS facility by mean of STH and CFD codes. Nucl. Eng. and Desing 409, 112349.

Stefanini, P., Galleni, F., Di Piazza, I., Pucciarelli, A., 2023. Liquid-Metal Thermal-Hydraulic Numerical Analyses in Support of the Upcoming CIRCE-THETIS Experimental Campaign. Nucl. Technol. https://doi.org/10.1080/00295450.2023.2189892.

THINS, https://cordis.europa.eu/project/id/249337/reporting.

A. Toti, J. Vierendeels, F. Belloni, "Coupled system thermal-hydraulic/CFD analysis of a protected loss of flow transient in the MYRRHA reactor", Annals of Nuclear Energy, Volume 118, 2018, Pages 199-211, ISSN 0306-4549, https://doi.org/10.1016/j.anucene.2018.03.032.

Uitslag-Doolard, H., Zwijsen, K., Roelofs, F., Stempniewicz, M.M., 2023. myMUSCLE, a New Multiphysics, Multiscale, Simulation Coupling Environment. Nucl. Sci. Eng. https://doi.org/10.1080/00295639.2022.2148809.

K. Van Tichelen, F. Mirelli, "Experimental investigation of steady state flow in the LBE-cooled scaled pool facility E-SCAPE", Proceedings of the 17th International Topical Meeting on Nuclear Reactor Thermal Hydraulics, Xi'an (China), September 3-8 (2017).

Victor Hugo Sanchez-Espinoza, 2023. Kanglong Zhang, Alejandro Campos Munoz, Michael Bottcher, "KIT Multi-scale thermal–hydraulic coupling methods for improved simulation of nuclear power plants". Nucl. Eng. Des. 405, 112218.

Zhang, X., Kanglong Zhang, V.H., Sanchez-Espinoza, H.C., 2020. Multi-scale coupling of CFD code and sub-channel code based on a generic coupling architecture. Ann. Nucl. Energy 141, 107353.

K., Zhang, "The multiscale thermal-hydraulic simulation for nuclear reactors: A classification of the coupling approaches and a review of the coupled codes" International Journal of Energy Research, 2'2': 44:3295-3315. DOI: 10.1002/er5111.

Zou, Z., Shen, C., Zhang, X., Wang, S., Chen, H., 2020. 3D thermal hydraulic characteristics analysis of pool-type upper plenum for lead-cooled fast reactor with multi-scale coupling program. Nucl. Eng. .Des 370, 110892.